Transparent and conductive silver nanowires networks printed by laser-induced forward transfer

P. Sopeña [a),b)], P. Serra [a),b)], J.M. Fernández-Pradas*[a),b)]

[a)] Department of Applied Physics, Universitat de Barcelona, Martí i Franquès 1, 08028, Barcelona, Spain

[b)] Institute of Nanoscience and Nanotechnology (IN2UB), Universitat de Barcelona, Av. Diagonal 645, 08028, Barcelona, Spain

* corresponding author: email: jmfernandez@ub.edu

Tel: +34 934039216

Abstract

Networks of silver nanowires (Ag-NWs) can be electrically conductive and optically transparent at the same time. Thus, Ag-NWs are promising candidates for substituting transparent and conductive oxides like indium-tin-oxide. Direct-write methods for printing patterns are suitable in order to reduce the amount of material used with respect to actual deposition methods on large areas that require post-processing steps.

In this work, we study the laser-induced forward transfer of Ag-NWs with the aim of printing conductive patterns that appear invisible at naked eye. A Nd:YAG laser system delivering 150 ns pulses at 1064 nm wavelength was coupled with a scan head for printing the Ag-NWs at different pulse energies (0.20-0.45 mJ).

It has been found that the area coverage of Ag-NWs, which is directly related with the optical an electrical properties of the patterns, increases as the laser pulse energy increases. A sheet resistance of 140 Ω/sq is reached when printing at the highest pulse energy tested. As a proof-of-concept, we printed simple circuits with a pair of invisible

electrodes connecting an LED on glass with a transmittance of 98.8 %, a haze of 0.5 %, a reflectance below 0.1 % and a sheet resistance of 340 Ω/sq.

Keywords: Laser-induced forward transfer; silver nanowires; transparent electrodes, printed electronics

1. Introduction

Transparent and conductive materials are required for the operation of modern devices such as touch-screens, LCD panels, OLEDs, solar cells or transparent heaters [1]. Up to the present, most of these materials are transparent conductive oxides (TCOs), with indium tin oxide (ITO) being the most widely used. However, TCOs are ceramic materials that are brittle and need to be deposited with methods requiring high-vacuum [1]. For this reason, new materials such as graphene, metallic nanowires or carbon nanotubes are being explored as an alternative to TCOs for the fabrication of transparent electrodes [2].

In the case of metallic nanowires materials, the strategy for reaching conductivity and transparency at the same time stands in the formation of a 2D connected network allowing the conduction of electrons and the transmission of light [1, 3]. The top conductive property of silver makes silver nanowires (Ag-NWs) networks to become one of the best future options for substituting ITO in transparent and conductive electrodes [2, 4]. One of the advantages of Ag-NWs in front of TCO is their flexibility, which allows their use on curved surfaces and on flexible substrates that are becoming more and more usual in the electronics industry [5]. Moreover, they are compatible with roll-to-roll [5-7], low-cost and large area deposition methods [1-3, 8, 9].

The usual strategy for producing transparent electrodes of Ag-NWs consists on depositing a layer of Ag-NWs on a whole area and then defining the geometry of the

electrodes by a posterior processing of the deposited material [10]. In this way, no contrast is visible, since all the surface is covered by Ag-NWs and the electrodes remain invisible. However, this strategy implies a waste of material in the areas where no electrical conduction is needed. Thus, digital printing strategies for directly depositing Ag-NWs only where required would save material and time. This has been tried with ink-jet printers [11]. However, a previous sonication of the ink is necessary before printing in order to reduce the length of the Ag-NWs and avoid clogging of the nozzle. This length reduction is detrimental for the properties of the Ag-NWs networks [12], since higher densities are required for getting equivalent conductive properties, what results in reducing the optical transmittance of the network.

Lasers are being used for processing already deposited Ag-NWs. Their most common application is for removing already deposited material and delimiting the electrodes geometry by directly focusing the laser beam in the Ag-NWs layer [10, 13-16]. Lasers have been also used for selectively sintering previously deposited Ag-NWs [17-19]. In this case, the laser is used for welding the already deposited Ag-NWs between them, promoting a significant reduction of the contact resistance between wires and consequently the resistance of the irradiated area. However, this is a delicate process where an excess of laser intensity can lead to the transformation of the Ag-NWs into nanoparticles that would cause the destruction of the conductive paths and a sudden increase of the resistance [20]. In a more sophisticated application, a two-laser beam technique combining ultrashort and CW lasers has been used for directly fabricating single Ag-NWs [21, 22]. Now, we propose to use lasers for selectively printing Ag-NWs by using the laser-induced forward transfer (LIFT) technique [23]. For this, typically a pulsed laser is focused in the interface between a thin layer of the material to be printed (donor layer) and the substrate supporting it (donor substrate). The absorption of the

laser pulse energy promotes the formation of a vapor bubble near the interface that expands and pushes the material in front of it. For liquid layers, this promotes the ejection of part of the donor layer in the form of jets that propagate forward to the acceptor substrate where the liquid is deposited [24].

The possibility of LIFT for printing inks digitally in a large range of viscosities (1 - 1000 mPa·s) [25] is one of its major advantages in front of other well-established printing techniques like screen-printing, slot die or inkjet. LIFT allows to print inks with high solid content that would clog the printing heads of other direct-write printing techniques. The low restrictions in the ink formulation allows the use of cheaper inks and avoid the use of toxic or contaminant solvents, which, in addition to the above commented material saving as a direct-write technique, has environmental and economical benefits [26]. With resolutions of 300 dpi and 600 dpi, similar to other existing printing methods [27], estimated costs of printing [26] approaches the cost of mass production techniques like rotogravure, keeping the costs independent of the number of runs.

The absence of nozzle makes LIFT a very interesting approach for printing high-aspect ratio nanostructures. Indeed, it has been already demonstrated useful for printing carbon nanotubes [28-30] and carbon nanofibers [31, 32]. In a previous work, LIFT was used for printing electrodes of Ag-NWs embedded in a protecting binder matrix on a flexible substrate [33]. In that case, the Ag-NWs were transferred together with the binder matrix through the approximation of LIFT from solid donor layers. The binder matrix was required to prevent the Ag-NWs breaking during the transfer process. Flexible and stretchable electrodes with conductive properties were printed. However, the best transmittance of conductive patterns was 80%, which could be considered transparent but are clearly visible when printed on transparent substrates such as glass.

Recently, pixels with AgNWs have been directly transferred by LIFT from a donor layer that has been left dry before the printing process [34]. The transfer is performed with the donor and receiving substrates in low vacuum contact. In this case the transmittance achieved is near 90%.

In this work we explore the printing of Ag-NWs by LIFT from a liquid donor layer with the challenge to produce invisible conductive patterns on transparent substrates. The main objective of this research is to demonstrate the potential of LIFT for directly printing Ag-NWs only where they are required without further scribbing or trimming processes [10, 13], with the associated saving of material and time that is of interest from the environmental and economical point of view. A commercial ink containing Ag-NWs is used and directly applied as donor layer. The LIFT approximation with liquid donor layers has been demonstrated soft enough to transfer even very delicate biomolecules such as DNA or proteins [35-38]. Consequently, Ag-NWs should not suffer any damage during the printing process.

2. Experimental

A Nd:YAG laser (Baasel Lasertech, LBI-6000) coupled to a scanner head of galvanometric mirrors was used to perform LIFT. The laser was operated at the fundamental wavelength (1064 nm), in pulsed mode, at a repetition rate of 1 kHz, in all the experiments presented in this work. The pulse duration using these parameters was around 150 ns. The energy of the pulses ranged between 0.10 and 0.45 mJ by modifying the current of the pumping lamp. The laser beam has a Gaussian intensity profile and it was focused by an f-theta lens of 100 mm focal length. The beam diameter in the focusing plane for LIFT configuration was measured as 80 μm . The scanner head moved the beam at a speed of 800 mm/s for printing isolated pixels and of 200 mm/s for

printing continuous patterns such as lines and areas. Hence, as the laser was always firing pulses at 1 kHz, the separation between consecutive pixels was 200 μm in printed patterns.

The ink used as donor was the Ag-NWs suspension ClearOhm™ from Cambrios with a viscosity in the range of 15-25 mPa·s. The donor substrates were borosilicate glass slides (25×75×1 mm^3) with a 50 nm thick film of Ti (Deposition Research Lab, Inc.) acting as absorption layer for the laser radiation. The donor films were prepared by spreading 40 μl of the ClearOhm™ ink on top of the Ti absorption layer by means of a doctor blade coater obtaining a thickness of around 20 μm. The receiving substrates were microscope glass slides placed in front of the receiving substrate surface at a distance of 150 μm.

After deposition, the printed patterns were submitted to a bake process in an oven at 200 ^oC during 400 s in order to improve the contact between nanowires. Thus, the electrical resistance of the networks was reduced. Although the process was not optimized, the conditions used do not produce the spheroidization of the nanowires that can be induced by too high temperatures or too long times [12]. The morphology of the samples was observed by optical microscopy (Carl Zeiss AX10 Imager.A1) and scanning electron microscopy (SEM, JEOL J-7100) equipped with an energy dispersive detector for X-ray spectroscopy (EDS).

The resistance of the printed features was measured with a multimeter (Keithley 175A). With this value and the planar dimensions of the lines, the sheet resistance was then calculated in order to get a parameter independent of the size of the printed features [39].

Optical characterization was performed by a UV/Vis Spectrometer (Perkin Elmer - model Lambda 950) equipped with a 150 mm integrating sphere and reflectance accessories.

3. Results and discussion

The first experiments were devoted to characterize the morphology of individual pixels printed at different pulse energies. After printing, the pixels dry quickly (within 5 seconds) and can only be detected in the optical microscope with dark field illumination (Fig. 1a). Ag-NWs were only printed on the acceptor substrate at pulse energies above 0.20 mJ. Below this value, the donor material is not transferred to the acceptor substrate. Pixels are round and without evidence of splash and satellite droplets (a representative image is shown in Fig. 1a). The center of the pixels appear brighter with intense spots that correspond to spherical particles when looking at higher magnification. There is no sign of the coffee-ring effect in the dried pixels. It was shown that large aspect-ratio particles, like Ag-NWs, produce strong capillary interactions that reduce the effect of accumulating particles in the liquid-air contact line [40, 41]. These interactions, together with a fast-drying rate lead to a uniform distribution of the Ag-NWs along the whole pixel. The size of the pixels increases with pulse energy. The plot of the radius of the pixels at different pulse energies (Fig. 1b) shows a quite linear trend, from 130 μm at 0.20 mJ to 330 μm at the highest explored energy, 0.45 mJ. Similar values and a similar linear trend was observed when printing a silver nanoparticle ink with this laser system setup before [42]. The resolution could be improved by placing coated acceptor substrates for increasing the contact angle, using shorter laser pulses and smaller beam diameters [24].

The area coverage was evaluated from the optical microscope images at the highest magnification (×100) and corrected by taking into account the ratio between the apparent diameter of the Ag-NWs in the images and the real one. Its value increases with pulse energy until saturation at energies higher than 0.35 mJ (Fig. 1b). As the energy increases, a higher volume is transferred from the donor film [42]. Due to the linear ratio between the volume and the area of the base of a dome-shaped droplet, this would imply an increase of the area coverage for larger droplets printed at higher energies. However, on the basis of images of the transfer process taken with the same laser system and an ink with similar viscosity [42], it seems that, when the pulse energy is high enough, all the thickness of material in the donor film would be transferred and, consequently, the printed material in the acceptor substrate is replicating the surface coverage of the ink donor layer. Thus, at high pulse energies the area coverage cannot continue growing and remains constant.

Rectangular areas of 1.5×2.0 cm^2 were used for optical and electrical characterization of the printed Ag-NWs networks. These areas were printed by overlapping lines separated 200 μm, which is the same separation between consecutive printed pixels at the given scan speed. With this separation, the overlap between adjacent pixels is about 13% for the minimum pulse energy. This should guarantee continuity of the network for producing electrical conductive electrodes. Figure 2 shows a SEM image of the ink printed on the acceptor substrate with a detail of the large particles observed at the center of the pixels. It can be seen that Ag-NWs are randomly oriented, forming a connected network that would allow electrical conduction. The EDS analysis reveals that those large particles are titanium contamination coming from the donor absorbing layer (Fig. 2). These particles would correspond to the bright spots observed in the

center of the individual pixels (Fig. 1a) and are the result of the ablation of the donor absorbing layer.

The transmittance and sheet resistance values of the printed areas versus the laser pulse energy are plotted in Figure 3. The transmittance of the Ag-NWs networks is evaluated by comparing the transmittance spectrum of a printed sample with the transmittance spectrum of a clean acceptor substrate. The sample printed at 0.2 mJ has the best transmittance of the series reaching a value of 98.8%. When the pulse energy increases, the transmittance of the printed network decreases in an almost linear trend. For the maximum pulse energy tested in this work the transmittance is above 93%, which is more than acceptable for transparent electrodes. The sheet resistance decreases as the pulse energy for printing increases. The best value, 140 Ω/sq, is reached for the maximum pulse energy of 0.45 mJ. Transmittance and sheet resistance values are commonly related with the diameter and length of the nanowires and the areal density of the network [12]. In view that the morphology of the Ag-NWs is similar in all the printed samples, differences in the areal density should account for the trends observed for transmittance and sheet resistance. In one hand, higher areal densities allow more interconnections between the nanowires, improving the conductivity of the network, and consequently reducing the sheet resistance of the printed pattern. On the other hand, a higher transmittance is associated with lower areal densities.

The area coverage of the printed networks was evaluated from the optical microscope images with the same method used for individual pixels. The trend of the area coverage when increasing the pulse energy is very similar to the trend observed for the size of the pixels with the pulse energy (Fig.1b). The area coverage increases almost linearly with the pulse energy, in spite of the constant value observed when printing individual droplets (Fig. 1b). This fact is concomitant with the decrease in transmittance and sheet

resistance as the samples are printed at higher pulse energies and confirms the hypothesis that the trends observed are related with the areal density of the Ag-NWs network. The fact that the trends for the area coverage and pixel radius are so similar unveils some relationship between the density of the network and the size of the pixels at the pulse energy used for printing, as it can be observed in Fig. 4. In spite of the significant experimental error in the determination of the area coverage, the plotted points follow a good linear relationship with the pixel diameter. Taking into account that the area coverage found for single pixels is very similar, except when printing at the lowest pulse energy (Fig. 1b), and that the diameter of the pixels is larger than the separation distance between adjacent pixels, the increase in the area coverage must be related with the contribution of overlapping pixels. The overlapped area between two circles of radius *r* separated by a distance *d* can be calculated with the formula in eq. (1). With this, the overlap factor can also be calculated by considering the contribution of all the neighbor pixels that cover the same area. Fig. 4 shows how the overlap factor also follows a linear trend, especially for pixels much larger than the separation distance. Consequently, the increase in the area coverage with the pulse energy seems to be directly related with the increase in the size of the printed pixels and the corresponding overlap of successive printed pixels.

$$Overlapped\ area = 2r^2 \cdot \cos^{-1}\left(\frac{d}{2r}\right) - \frac{d}{2}\sqrt{4r^2 - d^2} \qquad (1)$$

However, the area coverage measured when printing areas by overlapping pixels is much lower than the area coverage resulting from multiplying the area coverage of single pixels by the overlap factor. This clearly indicates that the donor layer is suffering depletion of material. Taking into account that the diameter of the pixels is larger than the separation distance between consecutive pixels, and assuming the hypothesis that

almost all the material in the donor film is transferred, in every single pulse printing event, part of the material transferred is coming from a distance larger than the separation distance between consecutive pulses in the donor film. This material loss is partially refilled by liquid flow coming from the contiguous donor layer before the next pixel is printed.

In spite of the presence of contamination Ti particles coming from the absorbing donor layer, patterns of Ag-NWs can be printed with very high transmittance (near 99%). However, invisibility of individual tracks or patterns does not only depend on their transmittance. The eye is capable of detecting very small changes in scattered light, and also reflected light, especially in dark background conditions [43, 44]. That is why the haze, that gives account of scattered light, and reflectance were also evaluated. Figure 5 shows plots of the haze and reflectance of the networks printed at different laser pulse energies. In all cases the values are low, between 0.5 % and 3.5 % for the haze and below 1.8 % for the reflectance. However, both of them grow when increasing the pulse energy. This trend would be concomitant with the fact that higher areal densities are printed at higher pulse energies. It is worth to state that at 0.2 mJ the haze value is only 0.5 % and the reflectance 0.07%. These really small haze and reflectance values, together with a transmittance of 98.8%, should lead to almost undetectable patterns.

A simple circuit with two Ag-NWs tracks was designed as a proof-of-concept for the LIFT printing of invisible electrodes on glass (Fig. 6a). Each track connects two square silver contacts that were also printed by LIFT from a Ag-ink donor layer [42]. These contacts were used for preventing the Ag-NWs tracks from wear when testing with the current probes. An LED (SMD) was soldered between the two tracks as a test of continuity and electrical conductivity. The printing parameters leading to the best optical properties (maximum transmittance, minimum haze and minimum reflectance)

were selected, considering that maximum invisibility is pursued and that the sheet resistance value is good enough for application in touch screens [3]. Hence, 0.2 mJ of pulse energy were used for printing the Ag-NWs tracks. A photograph of three samples of the test circuit is presented in Fig. 6b. The four electrodes and the LED of each sample are clearly visible, while the printed Ag-NWs cannot be seen at naked eye. When injecting current (like in the right sample), the LED lights on, clearly indicating the presence of the two conducting Ag-NWs tracks.

In spite of these encouraging results, the relationships between sheet resistance, transmittance and haze for the ClearOhm® ink deposited by spin-coating or roll-to-roll slot-die coating under optimized conditions [5] are better than those obtained in this work. Therefore, there is still room for improving the performance of Ag-NWs printed by LIFT. Probably, the detected contamination of Ti (a material with lower conductivity than Ag) coming from the absorbing layer is negatively affecting the sheet resistance. The Ti particles may act as high contact resistance points between Ag-NWs. Their presence on the substrate can also difficult the planar connection between nanowires. LIFT with laser wavelengths in the UV or with ultrashort laser pulses can be used for printing without absorption layer and, thus, circumvent the contamination issue. The bake process is also a delicate point that must be optimized in order to reach even better results [12].

4. Conclusion

The results of this study demonstrate that conductive and transparent patterns of Ag-NWs can be printed by LIFT using an ink as donor layer. Compared to other printing techniques such as screen or inkjet printing, LIFT has proven feasible for depositing those large Ag-NWs for producing transparent electrodes in a digital manner.

The areal density of Ag-NWs in individual pixels is almost independent of the laser pulse energy used because all the thickness of the donor film is transferred to the printed pixels. However, the areal density can be increased in printed patterns by increasing the pulse energy. This has been directly related with a higher overlap between neighbor pulses. Consequently, better sheet resistance values are obtained when printing at higher pulse energies. On the contrary, higher transmittance, lower haze and lower reflectance values can be reached by decreasing the laser pulse energy.

As a proof-of-concept conductive electrodes were printed on glass with a transmittance of 98.8%, very low haze (0.5%) and low reflectance (0.07%). Owing to these excellent optical properties, the electrodes printed by LIFT are invisible to the eye under normal lighting conditions.

Acknowledgement

This work was funded by the AEI of the Spanish Government (Projects TEC2014-54544-C2-1-P, TEC2015-72425-EXP and TEC2017-83301-P).

References

[1] T. Sannicolo, M. Lagrange, A. Cabos, C. Celle, J.-P. Simonato, D. Bellet, Metallic nanowire-based transparent electrodes for next generation flexible devices: a review, Small 12 (2016) 6052–6075.

[2] S. De, J.N. Coleman, The effects of percolation in nanostructured transparent conductors, MRS Bull. 36 (2011) 774-781.

[3] L. Hu, H. Wu, Y. Cui, Metal nanogrids, nanowires, and nanofibers for transparent electrodes, MRS Bull. 36 (2011) 760-765.

[4] S. De, T.M. Higgins, P.E. Lyons, E.M. Doherty, P.N. Nirmalraj, W.J. Blau, J.J. Boland, J.N. Coleman, Silver nanowire networks as flexible, transparent, conducting films: extremely high DC to optical conductivity ratios, ACS Nano 3 (2009) 1767–1774.

[5] M. Spaid, Wet-processable transparent conductive materials, Inf. Disp. 28 (2012) 10-15.

[6] S.J. Lee, Y-H. Kim, J.K. Lim, H. Baik, J.H. Park, J. Lee, J. Nam, J.H. Park, T-W. Lee, G-R. Yi, J.H. Cho, A roll-to-roll welding process for planarized silver nanowire electrodes, Nanoscale 6 (2014) 11828.

[7] D. Angmo, T.R. Andersen, J.J. Bentzen, M. Helgesen, R.R. Søndergaard, M. Jørgensen, J.E. Carlé, E. Bundgaard, F.C. Krebs, Roll-to-Roll printed silver nanowire semitransparent electrodes for fully ambient solution-processed tandem polymer solar cells, Adv. Funct. Mater. 25 (2015) 4539-4547.

[8] J. Liang, K. Tong, Q. Pei, A water-based silver-nanowire screen-print ink for the fabrication of stretchable conductors and wearable thin-film transistors, Adv. Mater. 28 (2016) 5986-5996.

[9] F. Hoeng, A. Denneulin, N. Reverdy-Bruas, G. Krosnicki, J. Bras, Rheology of cellulose nanofibrils/silver nanowires suspension for the production of transparent and conductive electrodes by screen printing, Appl. Surf. Sci. 394 (2017) 160–168.

[10] W. Gaynor, S. Hofmann, M.G. Christoforo, C. Sachse, S. Mehra, A. Salleo, M.D. McGehee, M.C. Gather, B. Lüssem, L. Müller-Meskamp, O. Peumans, K. Leo, Color in the corners: ITO-free white OLEDs with angular color stability, Adv. Mater. 25 (2013) 4006-4013.

[11] D.J. Finn, M. Lotya, J.N. Coleman, Inkjet printing of silver nanowire networks, ACS Appl. Mater. Interfaces 7 (2015) 9254–9261.

[12] M. Lagrange, D.P. Langley, G. Giusti, C. Jiménez, Y. Bréchet, D. Bellet, Optimization of silver nanowire-based transparent electrodes: effects of density, size and thermal annealing, Nanoscale 7 (2015) 17410-17423.

[13] T. Pothoven, Laser patterning of silver nanowire, Inf. Disp. 28 (2012) 20-24.

[14] J.W. Yoon, W.S. Chang, S.H. Cho, Laser direct patterning of AgNW/CNT hybrid thin films, Opt. Lasers Eng. 73 (2015) 40–45.

[15] H. Oh, J. Lee, J-H. Kim, J-W. Park, M. Lee, Fabrication of invisible Ag nanowire electrode patterns based on laser-induced Rayleigh instability, J. Phys. Chem. C 120 (2016) 20471-20477.

[16] B. Yoo, Y. Kim, C.J. Han, M.S. Oh, J-W. Kim, Recyclable patterning of silver nanowire percolated network for fabrication of flexible transparent electrode, Appl. Surf. Sci. 429 (2018) 151-157.

[17] J.A. Spechler, C.B. Arnold, Direct-write pulsed laser processed silver nanowire networks for transparent conducting electrodes, Appl. Phys. A 108 (2012) 25–28.

[18] J. Lee, P. Lee, H. Lee, D. Lee, S.S. Lee, S.H. Ko, Very long Ag nanowire synthesis and its application in a highly transparent, conductive and flexible metal electrode touch panel, Nanoscale 4 (2012) 6408-6414.

[19] J.A. Spechler, K.A. Nagamatsu, J.C. Sturm, C.B. Arnold, Improved efficiency of hybrid organic photovoltaics by pulsed laser sintering of silver nanowire network transparent electrode, ACS Appl. Mater. Interfaces 7 (2015) 10556−10562.

[20] H. Oh, J. Lee, M. Lee, Transformation of silver nanowires into nanoparticles by Rayleigh instability: Comparison between laser irradiation and heat treatment, Appl. Surf. Sci. 427 (2018) 65-73.

[21] G-C. He, M-L. Zheng, X-Z. Dong, F. Jin, J. Liu, X-M. Duan, Z-S. Zhao, The conductive silver nanowires fabricated by two-beam laser direct writing on the flexible sheet, Scientific Reports 7 (2017) 41757.

[22] G-C. He, X-Z. Dong, J. Liu, H. Lu, Z-S. Zhao, Investigate the electrical and thermal properties of the low temperature resistant silver nanowire fabricated by two-beam laser technique, Appl. Surf. Sci. 439 (2018) 96-100.

[23] A. Piqué, P. Serra, Laser printing of functional materials: 3D microfabrication, electronics and biomedicine, Weinheim, Wiley-VCH, 2018.

[24] J.M. Fernández-Pradas, C. Florian, F. Caballero-Lucas, P. Sopeña, J.L. Morenza, P. Serra, Laser-induced forward transfer: Propelling liquids with light, Appl. Surf. Sci. 418 (2017) 559-564.

[25] V. Dinca, A. Patrascioiu, J.M. Fernández-Pradas, J.L. Morenza, P. Serra, Influence of solution properties in the laser forward transfer of liquids, Appl. Surf. Sci. 257 (2012) 9379–9384.

[26] G. Hennig, T. Baldermann, C. Nussbaum, M. Rossier, A. Brockelt, L. Schuler, G. Hochstein, Lasersonic® LIFT Process for Large Area Digital Printing, J. Laser Micro/Nanoeng. 7 (2012) 299-305.

[27] S. Khan, L. Lorenzelli, R.S. Dahiya, Technologies for printing sensors and electronics over large flexible substrates: a review, IEEE Sensors J. 15 (2015) 3164-3185

[28] A. Palla-Papavlu, M. Dinescu, A. Wokaun, T. Lippert, Laser-induced forward transfer of single-walled carbon nanotubes, Appl. Phys. A 117 (2014) 371-376.

[29] C. Constantinescu, S. Vizireanu, V. Ion, G. Aldica, S. D. Stoica, A. Lazea-Stoyanova, A.P. Alloncle, P. Delaporte, G. Dinescub, Laser-induced forward transfer of carbon nanowalls for softelectrodes fabrication, Appl. Surf. Sci. 374 (2016) 49-55.

[30] A. Palla-Papavlu, M. Filipescu, S. Vizireanu, L. Vogt, S. Antohe, M. Dinescu, A. Wokaun, T. Lippert, Laser-induced forward transfer of hybrid carbon nanostructures Appl. Surf. Sci. 374 (2016) 312-317.

[31] P. Sopeña, J. Arrese, S. González-Torres, J.M. Fernández-Pradas, A. Cirera, P.Serra, Low-cost fabrication of printed electronics devices through continuous wave laser-induced forward transfer, ACS Appl. Mater. Interfaces 9 (2017) 29412-29417.

[32] J.M. Fernández-Pradas, P. Sopeña, S. González-Torres, J. Arrese, A. Cirera, P. Serra, Laser-induced forward transfer for printed electronics applications, Appl. Phys. A 124 (2018) 214.

[33] T. Araki, R. Mandamparambil, D.M.P. van Bragt, J. Jiu, H. Koga, J. van den Brand, T. Sekitani, J.M.J. den Toonder, K. Suganuma, Stretchable and transparent electrodes based on patterned silver nanowires by laser-induced forward transfer for noncontacted printing techniques, Nanotechnology 27 (2016) 45LT02.

[34] F. Zacharatos, P. Karvounis, I. Theodorakos, A. Hatziapostolou, I. Zergioti, Single step laser transfer and laser curing of Ag nanowires: a digital process for the fabrication of flexible and transparent microelectrodes, Materials 11 (2018) 1036.

[35] P. Serra, M. Colina, J.M. Fernández Pradas, L. Sevilla, J.L. Morenza, Preparation of functional DNA microarrays through laser-induced forward transfer, Appl. Phys. Lett. 85 (2004) 1639-1641.

[36] J.A. Barron, H.D. Young, D.D. Dlott, M.M. Darfler, D.B. Krizman, B.R. Ringeisen, Printing of protein microarrays via a capillary-free fluid jetting mechanism, Proteomics 5 (2005) 4138-4144.

[37] V. Dinca, M. Farsari, D. Kafetzopoulos, A. Popescu, M. Dinescu, C. Fotakis, Patterning parameters for biomolecules microarrays constructed with nanosecond and femtosecond UV lasers, Thin Solid Films 516 (2008) 6504-6511.

[38] C. Boutopoulos, P. Andreakou, D. Kafetzopoulos, S. Chatzandroulis, I. Zergioti, Direct laser printing of biotin microarrays on low temperature oxide on Si substrates, Phys. Stat. Sol. A 205 (2008) 2505-2508.

[39] A. Kamyshny, S. Magdassi, Conductive nanomaterials for printed electronics, Small 10 (2014) 3515-3535.

[40] P.J. Yunker, T. Still, M.A. Lohr, A.G. Yodh, Suppression of the coffee-ring effect by shape-dependent capillary interactions, Nature 476 (2011) 308-311.

[41] X. Wang, G. Kang, B. Seong, I. Chae, H.T. Yudistira, H. Lee, H. Kim, D. Byun, Transparent arrays of silver nanowire rings driven by evaporation of sessile droplets, J. Phys. D: Appl. Phys. 50 (2017) 455302.

[42] P. Sopeña, J.M. Fernández-Pradas, P. Serra, Laser-induced forward transfer of low viscosity inks, Appl. Surf. Sci. 418 (2017) 530-535.

[43] C. Preston, Y. Xu, X. Han, J.N. Munday, L. Hu, Optical haze of transparent and conductive silver nanowire films, Nano Res. 6 (2013) 461–468.

[44] T. Araki, J. Jiu, M. Nogi, H. Koga, S. Nagao, T. Sugahara, K. Suganuma, Low haze transparent electrodes and highly conducting air dried films with ultra-long silver nanowires synthesized by one-step polyol method, Nano Res. 7 (2014) 236–245.

Figure Captions

Figure 1. (a) Dark field image of a single pixel printed with a pulse energy of 0.2 mJ. (b) Plot of the average radius of printed pixels (black circles) versus the laser pulse energy. The dashed line corresponds to the linear fit of the represented points. In the same plot, the calculated area coverage with Ag-NWs of the single pixels (red squares) is also represented.

Figure 2. SEM image of printed Ag-NWs on glass with detail of big particles. The EDS elemental analysis unveils the contamination with Ti particles coming from the absorbing layer.

Figure 3. Plot of the transmittance (black squares) and the sheet resistance (red circles) versus the laser pulse energy. Note that the sheet resistance axis is reversed, so lower sheet resistances values are on the top.

Figure 4. Plot of the area coverage (black squares) versus the single pixel diameter. The solid line corresponds to a linear fit of the points. The overlap factor (red circles) calculated from equation (1) is also represented in the plot in the right axis. A similar trend is found in both cases.

Figure 5. Plot of the haze (black squares) and reflectance (red circles) versus the laser pulse energy.

Figure 6. (a) Scheme of the circuit proposed to test the viability of LIFT for printing invisible electrodes on glass substrates. All the contacts and electrodes were printed by LIFT. The four Ag ink contacts were printed with an ink containing silver nanoparticles [41]. Two invisible tracks of Ag-NWs are printed at 0.2 mJ pulse energy between the Ag-NP ink contacts. An LED (SMD) was soldered between the upper contacts for testing the conductivity of the printed tracks. The lower contacts were used for injecting current. (b) Image of printed circuits on glass. The Ag-NWs tracks are invisible to the naked eye.

When injecting current (right circuit), the LED light is on confirming the conductivity and continuity of the tracks.

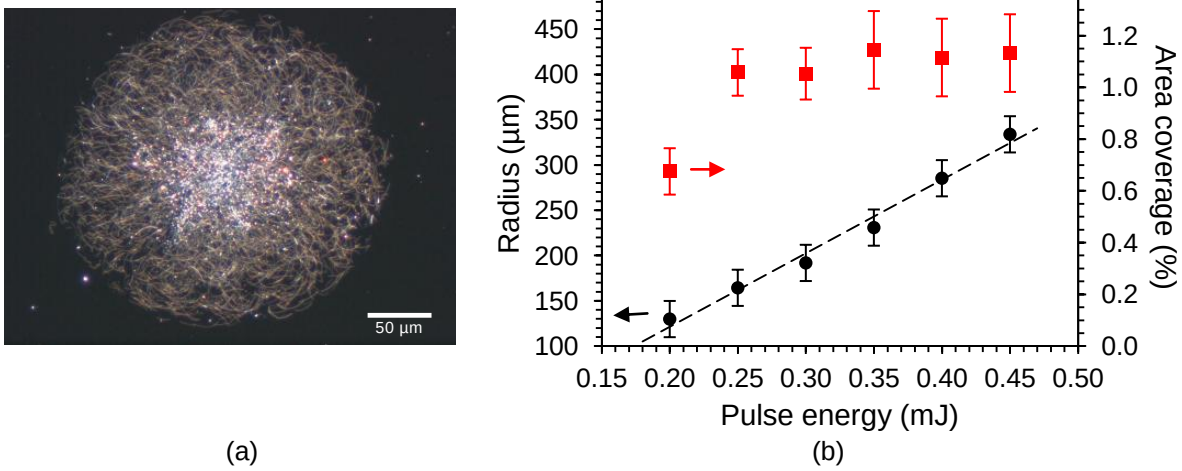
50 µm
Radius (µm)
Area coverage (%)
Pulse energy (mJ)
500
450
400
350
300
250
200
150
100
1.4
1.2
1.0
0.8
0.6
0.4
0.2
0.0
0.15
0.20
0.25
0.30
0.35
0.40
0.45
0.50

(a) (b)

Figure 1

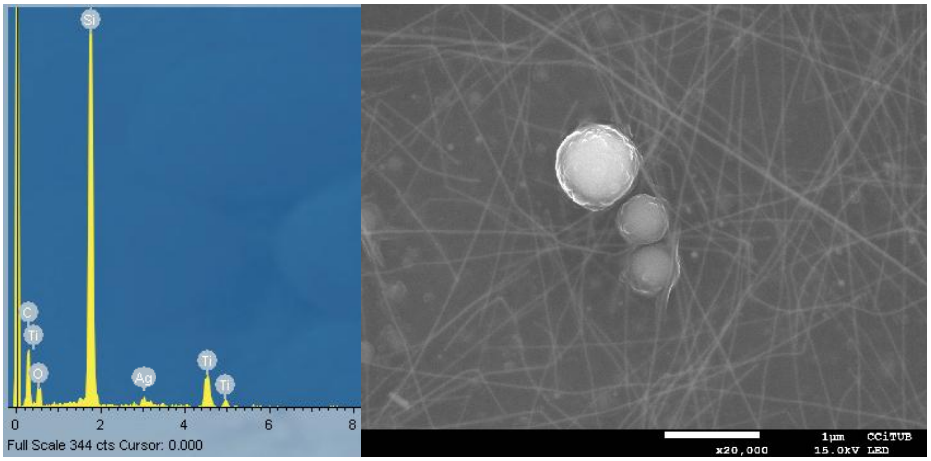
Si
C
Ti
O
Ag
Ti
Ti
0
2
4
6
8
Full Scale 344 cts Cursor: 0.000
1µm
x20,000
CCiTUB
15.0kV LED

(a) (b)

Figure 2

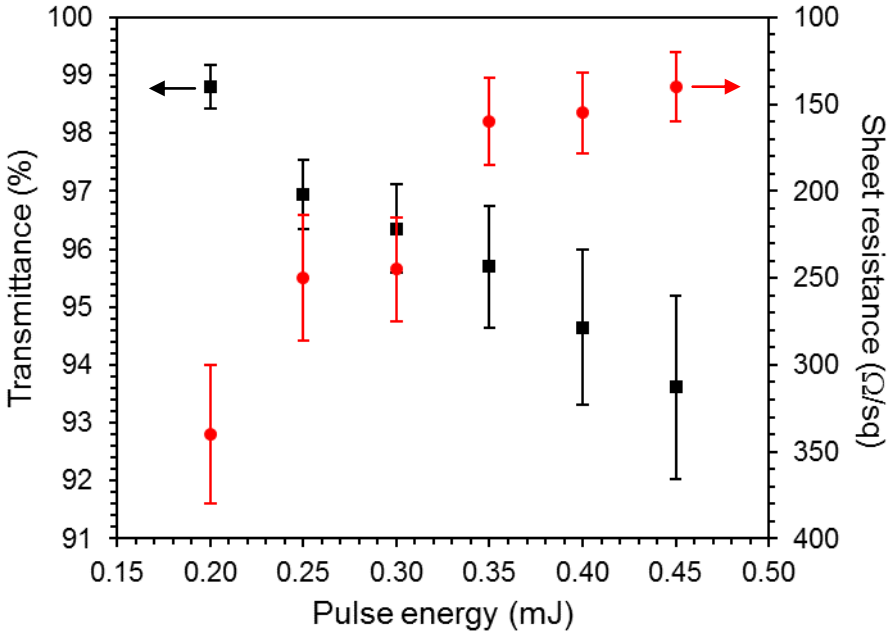
Transmittance (%)
Sheet resistance (Ω/sq)
Pulse energy (mJ)
100
99
98
97
96
95
94
93
92
91
150
200
250
300
350
400
0.15
0.20
0.25
0.30
0.35
0.40
0.45
0.50

Figure 3

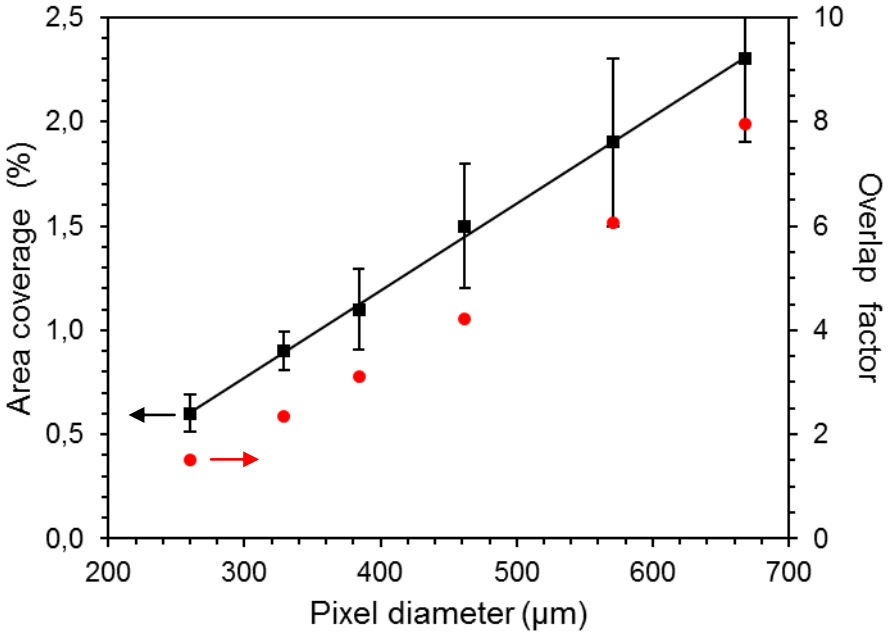
2,5
2,0
1,5
1,0
0,5
0,0
Area coverage (%)
10
8
6
4
2
0
Overlap factor
200
300
400
500
600
700
Pixel diameter (µm)

Figure 4

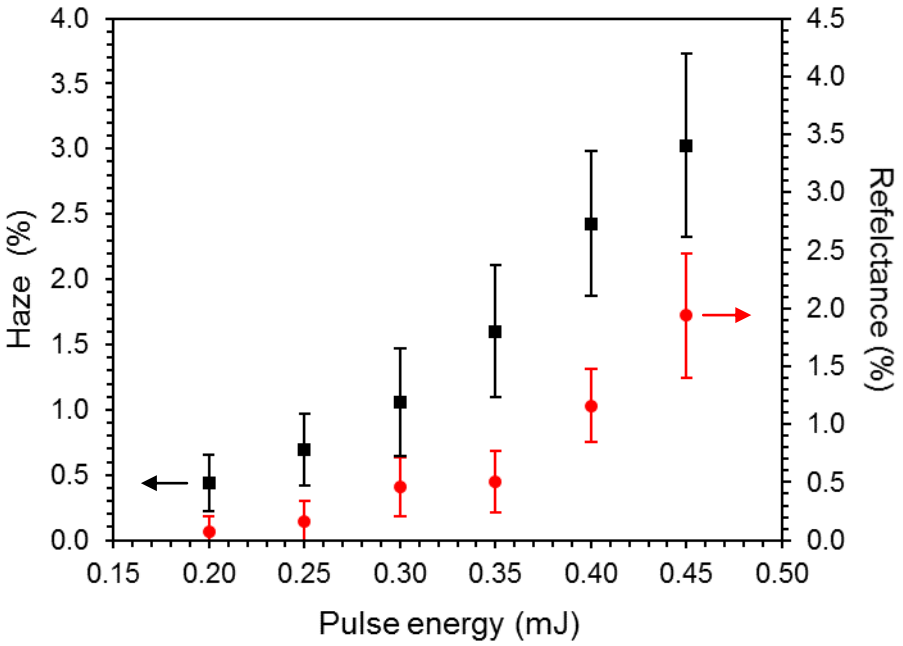
Haze (%)
Refelctance (%)
Pulse energy (mJ)
4.0
3.5
3.0
2.5
2.0
1.5
1.0
0.5
0.0
4.5
4.0
3.5
3.0
2.5
2.0
1.5
1.0
0.5
0.0
0.15
0.20
0.25
0.30
0.35
0.40
0.45
0.50

Figure 5

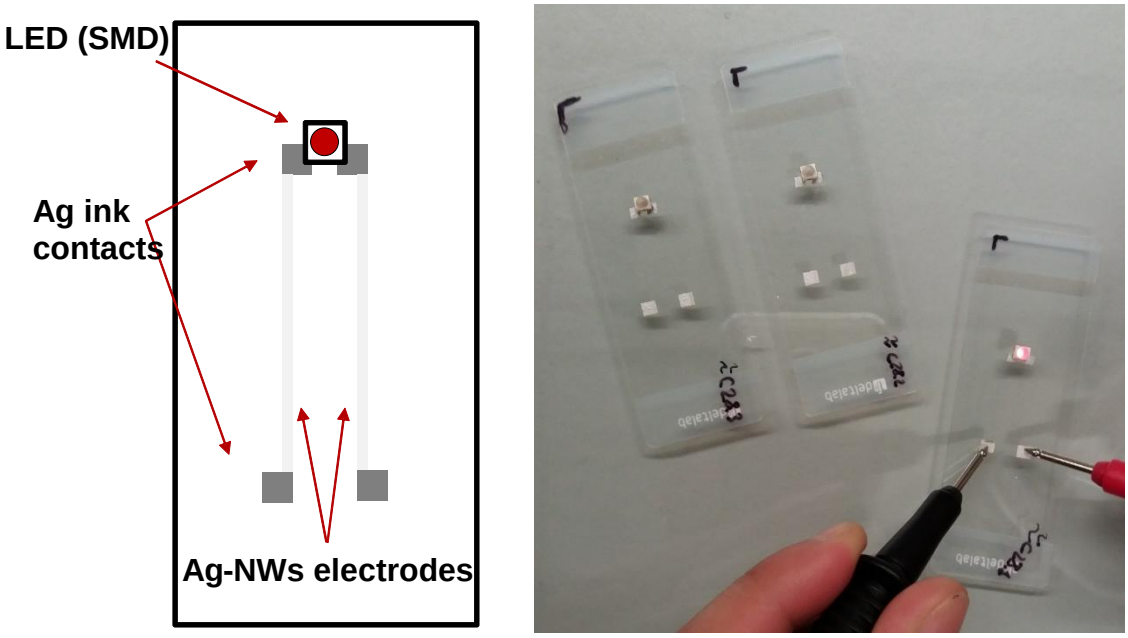

(a) (b)

Figure 6